Evaluation of Heartbeat Signal Extraction Methods Using a 5.8 GHz Doppler Radar System in a Real Application Scenario

C. Gouveia, *Student Member, IEEE*, D. Albuquerque, P. Pinho, *Senior Member, IEEE*, and J. Vieira

***Abstract*—Doppler-based radar systems have been seen as a promising tool to assess vital signs, since they are capable to monitor the respiratory and cardiac signal remotely, by measuring the chest-wall displacement. However, due to the spectral overlap of these signals, their proper separation is a challenging task. In this paper, we demonstrate the effectiveness of using Discrete Wavelet Transform in the cardiac signal extraction, by comparing this method with other approaches widely used in literature, namely a standalone Band-Pass Filtering, the Ensembled Empirical Mode Decomposition, the Continuous Wavelet Transform and the Wavelet Packet Decomposition. The comparison metrics were defined taking into consideration the heart rate computation accuracy, and also the peak detection consistency to further evaluate the Heart Rate Variability. The efficiency of those methods is also tested considering real application scenarios, characterized by non-controlled monitoring environment conditions and the ability to equally assess the vital signs of different subjects, regardless their physical stature.**

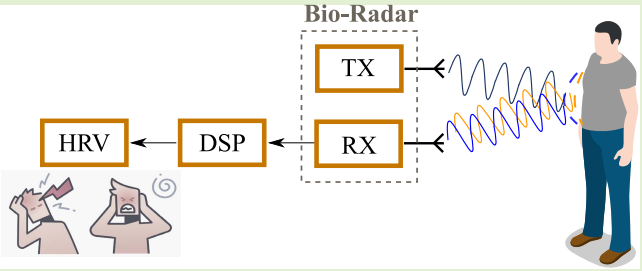

***Index Terms*— Doppler radar, continuous wave, vital signs, bio-radar, cardiac signal, discrete wavelet transform, wavelet packet decomposition, ensemble empirical mode decomposition, continuous wavelet transform.**

I. Introduction

THE non-contact vital signs monitoring using radar systems, also known as *Bio-Radar* systems, have been widely discussed in the research community. With this technology it is possible to keep track of the subjects' health condition, or even his/her psychological state remotely [1], [2], by assessing the cardiac and the respiratory signals. The bio-radar system stands out from the conventional sensors, such as the Electrocardiogram (ECG) and the Plethysmography, for being non-invasive, avoiding the direct contact with the subject. Thus, it has demonstrated to be a promising tool to revolutionize not only healthcare systems, but also the human lifestyle in general.

The bio-radar implementation has been reported using different radar front-ends [3]. Its operation principle is based on micro-Doppler radar, which uses electromagnetic waves to measure the chest-wall displacement during the cardiopulmonary activity [4]. For instance, Continuous-Wave (CW) radars transmit continuously an electromagnetic wave towards the subject's chest-wall. Then, the resulting echo is received and it consists on a phase modulated version of the transmitted signal, since the thoracic motion changes slightly the traveled path of the electromagnetic waves, as shown in Fig. 1. The received signal is a single signal containing both respiratory and cardiac components [4].

Despite its potential, the bio-radar implementation is not trivial due to several challenges. Among them, one can highlight the multipath environment or the signal interference due to random body motion. In [5] a deep review is performed concerning the random body motion and the self-motion produced by the radar handling, where it is highlighted the impact that the motion signals can have in the vital signs

Manuscript received January 31, 2022; revised February 25, 2022; accepted February 25, 2022. Date of publication March 3, 2022; date of current version April 14, 2022. This work was supported in part by the Fundação para a Ciência e Tecnologia (FCT) through Fundo Social Europeu (FSE) and by the Programa Operacional Regional do Centro through the Ph.D. Grant under Grant SFRH/BD/139847/2018 and in part by FCT/ Ministério da Ciência, Tecnologia e Ensino Superior (MCTES) through the National Fund and when applicable co-funded by the European Union (EU) Fund under Project UIDB/50008/2020-UIDP/50008/2020 and Project UIDB/05583/2020. The associate editor coordinating the review of this article and approving it for publication was Dr. Francesco Fioranelli. *(Corresponding author: C. Gouveia.)*

This work involved human subjects or animals in its research. Approval of all ethical and experimental procedures and protocols was granted by the Ethics and Deontology Committee of University of Aveiro, Portugal, under Application No. 29-CED/2021, and performed in line with the Declaration of Helsinki.

C. Gouveia, P. Pinho, and J. Vieira are with the Departamento de Eletrónica, Telecomunicações e Informática, Universidade de Aveiro, 3810-193 Aveiro, Portugal, and also with the Instituto de Telecomunicações, 3810-193 Aveiro, Portugal (e-mail: carolina.gouveia@ua.pt; ptpinho@av.it.pt; jnvieira@ua.pt).

D. Albuquerque is with the Centro de Investigação em Serviços Digitais CISeD, ESTGV—Politécnico de Viseu, 3504-510 Viseu, Portugal (e-mail: dfa@estgv.ipv.pt).

Digital Object Identifier 10.1109/JSEN.2022.3156474

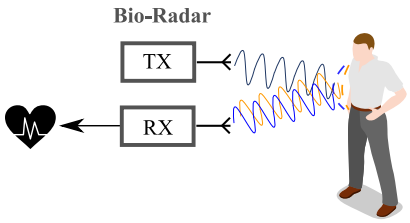

Fig. 1. CW bio-radar working principle.

accuracy. Even if the bio-signals are acquired in ideal and stationary conditions, the proper separation of the respiratory and cardiac signals is not trivial due to the spectral component proximity, to the harmonic superposition and also to the amplitude difference between both signals.

The first generation of bio-radars was proposed by Lin *et al.* [6] during the 70s decade. At this stage, authors could only detect the cardiac signal if the subject was in apnea. Since then, the research community has evolved and several solutions have been proposed to separate respiratory and cardiac signals, without requiring the subject to hold his breath [7]–[21].

Regarding the signal processing algorithms used for cardiac signal extraction, typically a band-pass or high-pass filter could be used as straightforward and direct approach to extract the heartbeat signal. However, filtering is not the most suitable technique, since the recovered cardiac signal might be distorted and loses resolution [7]. Furthermore, the filter performance is most likely compromised due to the respiratory signal nature. In fact, the respiratory signal cannot be seen as a monotone sinusoid, being rather an harmonic signal, with frequency components overlapping the cardiac signal. Due to this, it is not possible for a linear filter to completely separate both signals [7].

Recovering correctly the intact cardiac waveform, might be advantageous to identify certain health events. In addition to the heart rate, more information can be retrieved from this waveform, as the Heart Rate Variability (HRV). The HRV represents the change in the time interval between successive heartbeats [22]. HRV is a strong indicator of the cardiac vagal tone, which is highly related to several psychophysiological phenomena, such as our emotions, cognitive behaviors and it plays an important role on our health condition [22]. In order to compute the HRV parameters accurately, it is required to assess the Interbeats Interval (IBI) correctly. Most of the reported works focused in the HRV parameters via radar, apply band-pass filtering to remove the respiratory component and isolate the cardiac signal [11]–[13]. Additionally, in order to improve IBI results, in [11] filter bank is used with different center frequencies and in [13] the vital signs are acquired from the back, avoiding the high amplitude of the thoracic motion due to breathing. Despite the promising results obtained in [11]–[13] and due to the filter limitations aforementioned, there are different approaches that use methods based in signal decomposition and multi-resolution analysis, that can preserve the signal resolution.

In this work we compare the efficiency of different methods used in the literature for cardiac signal extraction, mostly using multi-resolution analysis and signal decomposition. The tested methods were a simple Band-Pass Filtering (BPF) for comparison purposes, the Ensemble Empirical Mode Decomposition (EEMD), the Discrete Wavelet Transform (DWT), the Wavelet Packet Decomposition (WPD) and the Continuous Wavelet Transform (CWT). The most efficient method should be capable to retrieve the cardiac waveform, leading to an accurate heart rate computation and simultaneously enabling the peak localization to further estimate the HRV parameters.

This method comparison is also performed considering the application in real scenarios, which can be challenging since it is usually performed in non-controlled environments (without laboratory conditions) during long time periods, and it encompasses inter-individual physical variability. In fact, each individual's physiological characteristics produces a varied radar cross-section and hence different amplitude chest-wall displacement [23]. Thus, for this work, a dataset was built with the vital signs of four different subjects with smaller and larger statures, and with a six-hour duration. The vital signs were acquired while the subjects were visualizing videos. These videos were used in our previous study [2], to induce three different emotions: happiness, fear and neutral condition, and thus achieve a higher variability on the heart rate, leading to more robust results.

To briefly summarize, our main contributions with this work, are the following:

- Carry out a method comparison to extract the cardiac signal waveform, considering non-controlled monitoring environments;
- Verify the cardiac peak location consistency and inspect if it is possible to compute HRV parameters;
- Study the results accuracy impact, when using subjects with different body statures.

This work is divided as the following: in Section II a literature overview is presented, mainly focused on the different methods that we aim to test in this work. Then, we present some highlights regarding the impact of operating bio-radars in real application scenarios. Our system setup is described in Section IV along with the procedure conducted during the signal acquisition stage and the signal processing algorithm implemented prior to the cardiac signal isolation. The methods implementation is described in Section V, where the considered evaluation metrics are also explained. Then, the obtained results and their discussion is presented in Section VI and leading to the conclusion in Section VII.

II. Literature Review on Multi-Resolution Analysis and Signal Decomposition

A. Wavelet Transform

In [10], [15], [18]–[21], [24], the wavelet transform is explored as an approach to extract the cardiac signal, since it can provide a multi-resolution perspective. In other words, long-time windows are applied to retrieve low frequency components and short-time windows are used for high frequency components.

Wavelets are functions with specific mathematical requirements, that can decompose the original signal into a set of signals [25]. For this purpose, a mother wavelet should be firstly selected and then scaled (by stretching or shrinking it) and compared with the input signal while shifting it over time.

The signal decomposition using wavelets can be performed using different analysis [26]. One can highlight the CWT, DWT and the WPD. For instance, CWT is widely used in time-frequency analysis and DWT is often used for denoise purposes [26]. The main difference between both is the scaling stage, since CWT provides a finer decomposition and DWT performs a dyadic scaling leading to a sparse decomposition.

Regarding DWT and WPD, both methods are similar to multi-rate filter banks (which provides the dyadic scaling feature). For instance, in DWT the original signal is decomposed in a certain number of scale levels [27]. On each scale level, the signal is simultaneously low-pass and high-pass filtered, being hereinafter downsampled by a factor of 2. The output of the high-pass chain consists on the detail coefficients $D(n)$ and the low-pass chain provides the approximation coefficients $A(n)$. The decomposition through levels is then performed, using $A(n)$ as the new input signal [27].

WPD is an extension of the DWT [27], where the $D(n)$ coefficients are also decomposed. In this way, WPD provides a better resolution in terms of frequency, as suggested in [27]. In [24] WPD is used to separate the respiratory and cardiac signals. The authors take advantage of the improved frequency resolution and perform a 6-level decomposition. Respiratory and cardiac signals are recovered through the combination of nodes containing the desired frequency band. CWT is used afterwards to obtain the cardiac rate, achieving an average absolute error varying between 1.69 and 3.22 beats-per-minute (BPM).

In the general literature, CWT is the most used method to recover the cardiac signal. More specifically, in [15] authors study which is the most appropriated scale factor to determine the IBI accurately. In [20], [21] CWT is used to improve the accuracy on the heart rate computation. First of all, [20] is focused on short-time applications. The authors compared the performance of their method with a conventional Fourier transform, achieving an average error reduction from 26.7% to 3.5 %. In [21] CWT is used to adapt the extraction properties to be suitable for different subjects in different monitoring scenarios. The authors obtained a Root-Mean-Squared Error (RMSE) varying between 0.1 and 4 BPM within the testing scenarios.

On the other hand, DWT is mostly used to denoise the cardiac signal, and not necessarily as a mean to isolate it. In [19] the authors study which are the best DWT features to denoise the cardiac signal acquired by a 5.8 GHz radar. They analyzed the Signal-to-Noise Ratio (SNR) of 115 potential functions, containing 6 wavelet families and 10 decomposition levels. They concluded that for the denoising purpose, Daubechies and Symlet wavelets with 9 vanishing moments are the most appropriated selection, considering 7 decomposition levels.

B. Empirical Mode Decomposition

The Empirical Mode Decomposition (EMD) technique consists on separating the input signal in a finite number of components [28], the so-called Intrinsic Mode Functions (IMFs). IMFs are obtained through a sifting approach, which consists in the following procedure [29]: firstly the lower and upper signal envelopes are obtained through cubic spline interpolations on local minima and maxima. Then, the mean value of both envelopes is subtracted from the input signal, and the same process is repeated until the IMF conditions are verified (see [28], [29]).

The signal decomposition in IMFs is performed iteratively, i.e. after finding the first IMF, this component is subtracted from the original signal and the result is submitted to the sifting process all over again. At the end, the original signal can be obtained through the sum of all IMFs plus a residual function.

EMD techniques are widely used in literature to extract the cardiac signal in the bio-radar context. For instance, in [16] the author used EMD to extract the heartbeat signals even in situations where the subject is randomly moving other body parts. In this case, the respiratory component is mitigated using a high-pass band filter and the EMD was applied afterwards. The authors tested the effectiveness of their method considering different amplitudes of body motion and obtained an RMSE between 0.6 to 1 BPM. On the other hand, it was demonstrated in [17] that it is possible to recover both bio-signals (respiratory and cardiac signals) concurrently using EMD. Herein the authors give an implementation example, where the cardiac signal was obtained through the first IMF isolation and the respiratory signal was reconstructed through the sum of the IMFs with more energy in the desired spectral component. The maximum error that the authors obtained in [17] was equal to 4.4 BPM.

More recently, the improved version of EMD, namely the EEMD was used in [10]. EEMD aims to solve inherent EMD issues, such as the mode mixing [30], which makes the physical meaning of an individual IMF unclear. For this purpose, the EEMD simulates successive observations of the same input signal, by adding white noise to it. Thus, each observation results from the noise addition with different characteristics. Adding noise will provide a relatively uniform reference scale distribution, which improves the EMD performance [30].

C. Methods Combination

The method proposed in [10] combines the DWT usage with EEMD. In this case wavelets threshold are used to denoise IMFs. Then, vital signs were accurately extracted by selecting the most appropriate IMFs, where the cardiac signal was recovered with an error equal to 0.014 BPM. The same method combination is proposed in [18] to separate bio-signals. Herein the authors state that the combination of both methods can provide results accurate enough to estimate the HRV. Since cardiac signals are tenuous in comparison with respiratory signals, in [18] wavelets are used due to their optimal resolution in time-domain for high-rate signals, and the EEMD is applied to help in signal reconstruction. Herein, the RMSE varied between 2.53 and 4.83%.

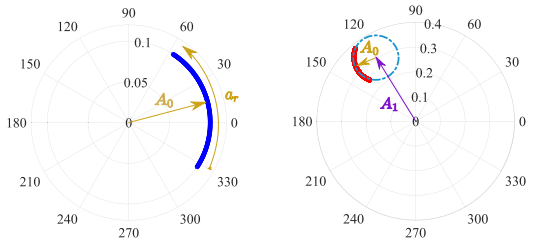

(a) Ideal case. (b) With parasitic reflections.

Fig. 2. Baseband signal represented in the complex plane.

III. Implications of Real Application Scenarios on Bio-Radar Signals

Generally in CW radars, signals are acquired by quadrature receivers, that perform a downconvertion to baseband using in-phase and quadrature demodulation. Thus, the signal processing is performed using complex signals. The received baseband signal can be represented by an arc projected in the complex plane, as depicted in Fig. 2a (neglecting the parasitic reflections).

Its mathematical form can be represented by equation (1) [5]:

$$g(n) = g_0(n) + g_1 = A_0 e^{j\varphi(n)} + A_1 e^{j\theta_1} \tag{1}$$

where, $g_0(n)$ represents the desired bio-signal and g_1 the sum of all parasitic reflections. Starting with the desired bio-signal, A_0 is the received signal amplitude (and the arc radius) and $\varphi(n)$ represents the phase change function according to the chest-wall motion. The phase change generates the arc depicted in Fig. 2a, which can be mathematically written as equation (2):

$$\varphi(n) = \theta_0 + \frac{4\pi a_r d(n)}{\lambda}, \tag{2}$$

where $\theta_0 = (4\pi d_o/\lambda) + \phi$, is the average distance traveled by the wave, considering the nominal distance between the radar and the target, d_o, the phase shift at the target's surface ϕ and the wavelength λ. Bio-signals are described by the $4\pi a_r d(n)/\lambda$ term, where $d(n)$ encompass both respiratory and cardiac signals. Bio-signals can be seen as periodical waveforms, being the respiratory signal the one with higher amplitude a_r. Thus, a_r corresponds to the arc length in the complex plane.

The parasitic reflections that occur in the monitoring environment can be described by g_1 component, from equation (1), where A_1 represents the amplitude of the parasitic reflections. For simplicity purposes, let us consider that the parasitic reflection occurs due to one stationary object, located at a distance d_1 from the radar. The phase shift on this object can be defined as $\theta_1 = (4\pi d_1/\lambda)$ and is also seen as an addition of complex DC component in the baseband spectrum. The resulting complex plane is depicted in Fig. 2b, where the DC component is perceived as DC offsets added to the arc center. Thus, the parameter A_1 dictates the distance from the arc center to the origin of the complex plane, and d_1 dictates the position of the arc center in the complex plane, i.e. its coordinates.

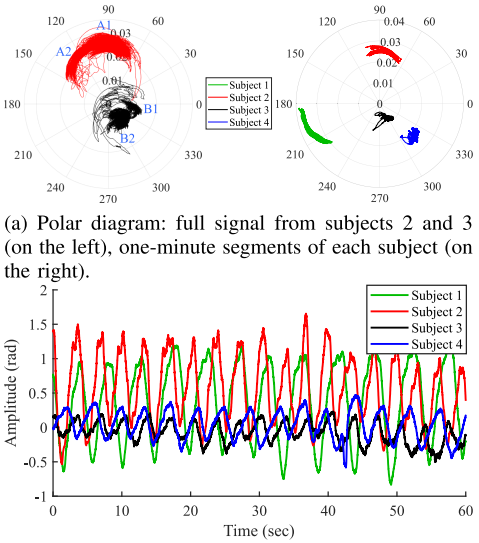

(a) Polar diagram: full signal from subjects 2 and 3 (on the left), one-minute segments of each subject (on the right).

(b) One-minute segments after vital signs recover.

Fig. 3. Received signal in a non-controlled environment.

In real application scenarios, this component might change over time if the subject under monitoring moves slightly uncovering different objects, or even if other targets located in the environment change their position. This means that the distance d_1 varies in time accordingly, leading to θ_1 and A_1 parameters to change as well. Hence, the parasitic component of the baseband signal should now be re-written as $g_1(n) = A_1(n)e^{j\theta_1(n)}$, with $\theta_1(n) = (4\pi d_1(n)/\lambda)$, which indicates that the DC offsets might also change over time [31].

In addition to the parasitic reflections, real application scenarios might also encompass low amplitude signals due to two reasons: the misalignment between the antenna beam and the chest-wall location that produces the maximum displacement when the subjects randomly moves, and the variety of the subjects' body statures which might also be related with the subject's gender. In [23] it is presented a correlation between anatomical differences relative to gender and the chest-wall displacement. Men's rib cage have a higher antero-posterior diameter and a larger cross-sectional area and volume. On the other hand, women have a disproportionately smaller rib cage comparing with men, and hence a lower cross-sectional area. In [23] it is also concluded that the men's lungs are bigger in absolute volume, which produces wider volume variations. This means that men might produce high amplitude signals (leading to higher length arcs a_r) and women lower amplitude ones.

Fig. 3 shows an example of some signals that might support the aforementioned hypothesis. These signals correspond to some samples acquired in the scope of this study. The subjects presented different physical characteristics, which were measured for control purposes, namely the height, their Body Mass Index (BMI) and their thoracic perimeter aligned with the diaphragm. Subject 1 and subject 2 presented higher reflection areas. They are males and have a thoracic perimeter equal to 90 cm and 96.5 cm, a height equal to 1.75 m and 1.76 m and a BMI of 22.20 and 27.44 kg/m^2, respectively. On the other

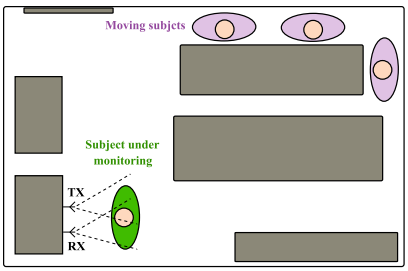

Fig. 4. Schematics of the monitoring scenario.

hand, subject 3 and subject 4 are females and have a narrower thoracic perimeter, namely 75 cm and 82 cm, a shorter stature, being 1.56 m and 1.50 m height and 25.07 and 18.70 kg/m^2 of BMI, respectively. Hence, these lower physical dimensions represent a decreased reflection area.

Fig. 3a shows the received signal projection in the complex plan. On the left, it is possible to observe the full raw signal obtained during a 30 minute acquisition, from subject 2 in red and from subject 3 in black. Herein, it is possible to observe that both subjects moved during the experiment which caused a DC offsets change. For instance, two distinct groups of arcs can be observed in subject 2, marked as A1 and A2. The DC offsets change is even more pronounced in the subject's 3 case, respectively marked as B1 and B2.

The signals samples of the Fig. 3a on the left side also shows a difference on the arcs length, that might be related with the size of the reflecting areas of both subjects. Fig. 3a on the right, presents the arcs corresponding to one-minute segments of all subjects. Once again, it is possible to observe the impact of the body statures differences, once subjects 1 and 2 produced a larger arc than subjects 3 and 4. Finally, the same effect is perceived in the extracted waveform present in Fig. 3b, after the Digital Signal Processing (DSP) algorithm, i.e. without the complex DC offsets and after the phase demodulation. Herein different amplitude signals were obtained.

IV. Hardware Description and Data Collection

In this work, a bio-radar prototype was used operating with CW at 5.8 GHz. Fig. 4 shows the schematics of the room used as non-controlled monitoring environment. The setup used was composed by a software-defined radio as RF front-end, namely the USRP B210 board from Ettus Research^{TM}. Two 2×2 antenna arrays were used for transmission and reception, respectively. These antennas have circular polarization and are crossed polarized to avoid the mutual coupling and to improve the path gain [32]. Both antennas have an half-power beamwidth of 40° approximately, and a gain equal to 11.6 dBi. The setup was operated with a transmitted power equal to 2 dBm.

As mentioned previously, the vital signs of four subjects were acquired, where two were males and the other two were females. The study was approved by the Ethics and Deontology Committee of University of Aveiro, Portugal (No.29-CED/2021) and an informed consent was obtained from all the subjects. The subjects were seated in front of the antennas at a distance of half meter and they were asked

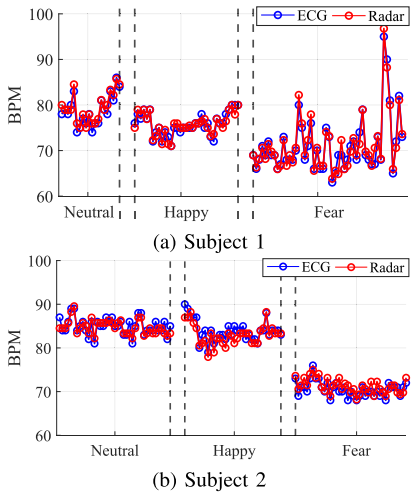

Fig. 5. BPM variation over time for different emotional conditions.

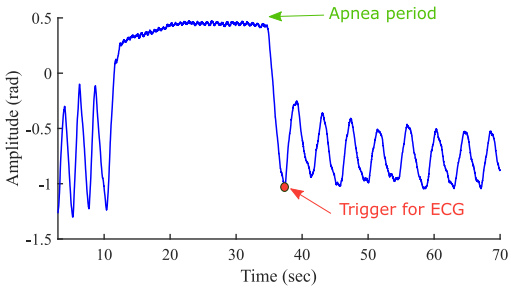

Fig. 6. Breathing pattern and trigger definition for signals synchronization.

to remain still as much as possible during the experiment. Subjects were monitored while they were watching videos, selected to induce three emotions [2]: happiness, fear and the neutral condition. The main goal of these videos was to take advantage of a wider variability in the heart rate caused by the emotions felt and also to account with the individual differences.

Fig. 5 shows an example of the number of BPM over time for two subjects. It varied from 65 to 95 BPM along with the different emotional conditions. Besides, each subject had a different reaction for each set of videos. These events led us to obtain unbiased and more robust results.

The experiment was conducted in different sessions occurring on separate days. Each session was dedicated to a different emotion and it was composed by a baseline period of 5 minutes approximately, and an inducing moment that lasted around 20-30 minutes. The collected dataset has a total duration of 367 minutes (around 6 hours). The vital signs were acquired simultaneously, using our bio-radar prototype and the BITalino (r)evolution BT board for the ECG signal [33].

In order to synchronize both signals, the subjects were asked to perform a breathing pattern composed by three deep breaths, an apnea period of 10 seconds and a slow exhale as depicted in Fig.6. Then, immediately before the next inhale, the subject pushed a trigger button to start the ECG acquisition.

Our study aims to compare different methods for the cardiac signal extraction and verify their performance in

real application scenarios, which implies that: i) the monitoring environment cannot be controlled, ii) the population under monitoring can encompass subjects with different body statures and iii) the signal amplitude might change during long term acquisitions, because it is impossible to remain completely still and keep the same body position.

In order to address to the aforementioned issues, the signals of all subjects were acquired inside a conventional room (outside the laboratory environment), with other subjects inside the room at the same time, but out of the antennas range. Since the signals are acquired during 30 minutes, it is expected that the subject under monitoring move according to his/her reaction to the videos or even to adjust his/her position, seeking for a comfortable posture. All these conditions could generate a time varying multipath environment that eventually changes the complex DC offsets accordingly, as it was previously observed in Fig. 3a.

Bio-radar signals were acquired using the GNU Radio Companion software, with a sampling frequency equal to 100 kHz. After receiving the signal, it was processed using MATLAB in order to remove the complex DC component and to recover the vital signs. This procedure is explained on detail, in the next sub-section.

A. Processing Signal Algorithm

Taking into account the effects observed in the real life signals, for instance as the ones depicted in Fig. 3a, the DSP algorithm presented in [31] was applied to recover the vital signs. This algorithm is robust to low amplitude signals and is implemented dynamically to encompass the DC offsets time variations.

Considering the arc shape that the baseband signal has in the complex plane (see Fig. 2b), one common method used in literature for the DC offsets compensation is the Park *et al.* method [34], which uses a circle fitting applied to the arcs to identify their center coordinates (which are the DC offsets values). Then, those coordinates can be subtracted from the remain signal, and the phase demodulation can be subsequently performed to recover vital signs, using the arctangent method [35]. However, the solution proposed by Park *et al.* is not successful when the signals are weak, since they lose their arc shape, being rather a cluster of disperse samples. In those cases, the fitting is performed considering that all radar samples form a circle, hence the coordinates estimation is often provided in the middle of the radar samples, pushing the arc to oscillate around the complex origin and providing an incorrect arctangent result. The algorithm proposed in [31] uses a customized cost function minimization, by setting the searching area outside the radar samples. With the arc center solution located outside the radar samples, the signal can be properly re-centered around the origin.

Furthermore, the algorithm from [31] is applied dynamically over time, in order to encompass eventual DC offsets changes that might occur due to body motion, for instance. For this purpose, the DC offsets are estimated using an overlapped windowing approach. A vector is created with the successive estimations of each window, which is then interpolated to assign a DC offset coordinate pair to each radar sample. The DC offsets are removed smoothly after subtracting the interpolated vector from the radar signal.

As mentioned in [31], the algorithm presents some limitations. One is regarding the DC offsets solution obtained through the cost function minimization. The minimum zones can occur in both arc sides, i.e. inside and outside its concavity. Since different solutions are provided over time through the windowing approach, successive windows might present solutions in opposite sides of the arc, adding an undesired variability degree to the overall center estimation. In order to attenuate this effect, a Savitzky-Golay filter is applied to the coordinate vectors before interpolation. However, the Savitzky-Golay filter provides intermediate values between two opposite ones, which might affect the final aspect of the signal. In order to solve this problem, we used a median filter combined with an interpolation using the nearest value, which revealed being more effective and it could remove the DC offsets without altering the original signal.

Finally, on the ECG side, a 15^{th} order band-pass FIR filter with pass-band equal to 6-20 Hz, was applied to highlight the R-peak detection and remove noise [36], providing a better comparison tool.

V. Method Evaluation

A. Methods Description

Considering the state of the art presented in Section II, a total of six methods (M1 to M6) were tested, compared and discussed in this work: **M1**) Single BPF, **M2**) DWT followed by EEMD, **M3**) Standalone DWT, **M4**) Standalone WPD, **M5**) WPD followed by EEMD and **M6**) Standalone CWT.

Despite the presented disadvantages of BPF, it is still widely used in literature. Therefore we decided to include it as a standalone method and evaluate its performance as well. Additionally, we verified in preliminary tests that applying a BPF prior to any other method, attenuates the respiratory component and improves the algorithms performance. For this reason, the remain methods (M2 to M6) are applied after a band-pass filtering stage.

Each method was implemented using the following specifications:

1) BPF: This method consists only on a 100^{th} order band-pass FIR filter, with a pass band between 0.7 and 2 Hz. This filter order was selected because it provides around 10 dB attenuation over the respiratory frequency band.

2) DWT: In this work, DWT is implemented to directly retrieve the cardiac waveform, rather than denoising it. The wavelet coefficients are obtained using the maximal overlap discrete wavelet transform, implemented with *modwt* function from MATLAB, considering 7 decomposition levels, as recommended by [19]. For this purpose, a Daubechies with 4 vanishing moments was selected as mother wavelet by trial. Then, the resultant signal can be recovered from the wavelet coefficients using the *modwtmra* function from MATLAB. The output of this function consists on a set of signals, with different frequency components. Since our signals are analyzed with a sampling rate equal to 100 Hz, the cardiac component is mainly present in the

5^{th} and 6^{th} decomposition levels. Therefore, only the signals of these two levels are summed.

3) WPD: This method is similar to DWT. A decomposition tree can be obtained using the *wpdec* function of MATLAB, with the same mother wavelet used in DWT. In order to avoid redundancy and save computational resources, only the 8^{th} decomposition level was selected to inspect the nodes. This level was chosen by trial, since it was the one providing enough frequency discretization on the cardiac band. The cardiac signal was reconstructed using the coefficients of the nodes which had the desired frequency, and this was performed using the *wprcoef* function.

4) EEMD: In order to implement EEMD, the guidelines suggested in [30] were followed: White noise was added to the input signal, with an amplitude equal to $A_W = 0.4 \times \sigma(x(n))$, where $\sigma(x(n))$ denotes the standard deviation of input signal $x(n)$. The noisy signal was decomposed in IMFs afterwards and these steps were repeated a total of 100 times, using different noisy samples. At the end, it was obtained the ensemble of means from all IMFs. Once again, their frequency content is evaluated, to select the ones with the desired spectral component and then sum them to reconstruct the cardiac signal.

5) CWT: The CWT was performed using the Morlet wavelet with *cwt* MATLAB function, which is the option suggested by [15] and [20]. In this case, Daubechies was not used since orthogonal wavelets are designed for dyadic scales (which are more spaced comparing with the ones used in CWT, to reduce redundancy) [26]. The cardiac signal was recovered using the *icwt* function, which once again selects the coefficients correspondent to the desired frequency band.

All the decomposition methods reconstructed the cardiac signal by summing the sub-signals with a spectral content between 0.8 and 2.5 Hz.

B. Evaluation Metrics

During the data processing stage, one could observe that different body statures produced signals with different amplitudes. In our particular case, the male subjects produced signals with higher amplitude and better SNR, comparing with the signals generated by the female subjects. Hence, there was a necessity to divide the dataset in a short-version (SH) and full-version (FL), in order to perform a more controlled analysis. Thus, the SH dataset has 217 minutes and includes signals from subject 1 and subject 2. This dataset is analyzed primarily to define which is the best method to extract the cardiac signal properly. Conversely, the FL includes all the 367 minutes and it is analyzed afterwards, to understand the impact that lower amplitude signals have in the algorithms performance (produced by the females considered in this study). Each dataset was divided in one-minute segments.

The methods performance was evaluated in two metric levels, respectively. The first metric level was focused on the heart rate accuracy (in BPM). The heart rate was computed using a zero-crossing approach: firstly the zero-crossing intervals were identified and the maximum of each interval was computed, corresponding to a peak. The IBI was computed between peaks for each one-minute segments and a time threshold

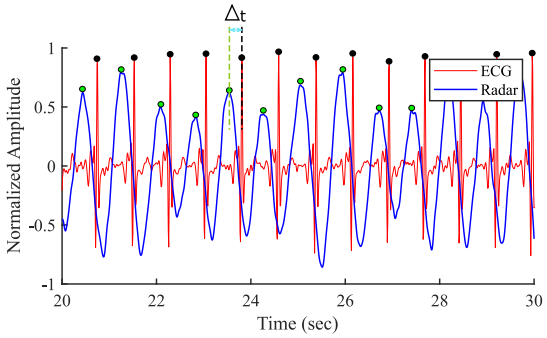

Fig. 7. ECG and radar signals superposition for peaks location evaluation, with the illustration of two peaks difference Δ_t.

was applied afterwards to remove outliers. The threshold was computed using half of the mean IBI of the full segment. The number of BPM was determined by the inverse of IBI values median.

The first metric level encompass the correlation coefficient between the radar cardiac signal and the ECG signal. A Bland&Altman (B&A) analysis is also performed in this scope [37]. Additionally, the coefficient of variation (CV) is also considered, to relate the variation between the radar and ECG measures with their mean value [38]. The absolute error in BPM was also evaluated and compared among the six methods. Finally, the computational speed and the results coherency in consecutive runs were also accounted.

The second metric level is related with the study of the peaks position in relation to the ECG signal. HRV parameters could be successfully computed in radar signals, if the peaks position and hence the IBI do not differ largely from the ECG. Thus, ECG and radar signals were superimposed and the peaks position was compared, as depicted in Fig. 7. It is expected that both signals are not perfectly synchronized, which means that a small lag offset can be acceptable. The most important aspect is to guarantee that this offset remains approximately constant over the segment. Furthermore, one should note that this delay may not last more than some milliseconds, so it is not expected to obtain biased results. For the heart rate case, since we are evaluating one-minute segments, the delay does not have impact in the total number of BPM because the delay duration is much less than the mean IBI.

Considering Fig. 7, some metrics were computed over the time difference between the ECG and radar peaks, marked as Δ_t: the average IBI of radar and ECG signals ($\overline{\text{IBI}}$), the standard deviation of such average IBI for both radar and ECG ($\sigma_{\overline{\text{IBI}}}$), the average value of the time difference between the radar and the closest ECG peak ($\overline{\Delta_t}$) and the standard deviation of such time difference ($\sigma_{\overline{\Delta_t}}$).

As we will see in the next section, the ECG results suggest a slight variability on the $\sigma_{\overline{\text{IBI}}}$, due to our psychophysiological behavior. This is the variation that induce the HRV parameters. The radar signals should vary in the same scale, to equally produce reliable results. Thus, the $\sigma_{\overline{\text{IBI}}}$ for radar is the first indicator of the peaks location consistency. Then, the remain metrics may justify such variation.

For the time difference $\overline{\Delta_t}$, the algorithm seeks for the closest ECG peak in relation to the radar peak under evaluation.

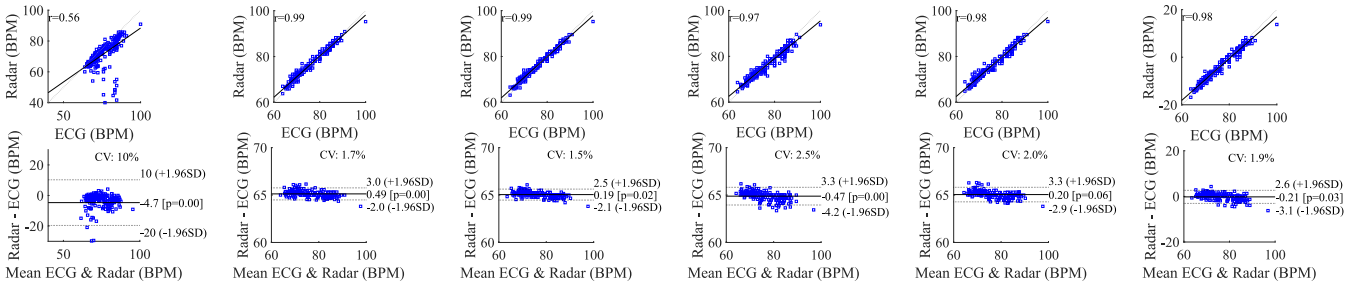

(a) BPF (M1) (b) DWT+EEMD (M2) (c) DWT (M3) (d) WPD (M4) (e) WPD+EEMD (M5) (f) CWT (M6)

Fig. 8. Correlation and B&A graphs for tested methods using the SH dataset.

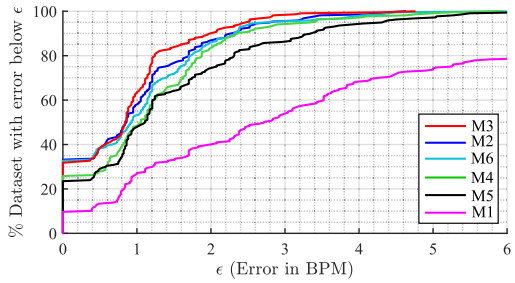

Fig. 9. Empirical cumulative distribution function of the BPM error for all methods using SH dataset.

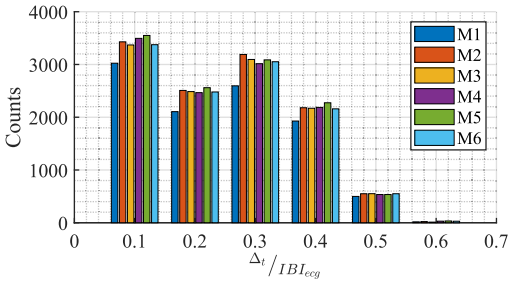

Fig. 10. Histogram with the distribution of Δ_t over ECG $\overline{\text{IBI}}$ using SH dataset.

The most important metric is the $\sigma_{\overline{\Delta_t}}$, which indicates the variation level of the peaks position in relation to the corresponding ECG peaks, and it should be the lowest as possible.

VI. Results Discussion

First of all, let us start with the SH dataset evaluation. Fig. 8 depicts the Correlation and the B&A graphs for all the six methods. Additionally Fig. 9 shows the error behavior for all methods. The results of such graphs are summarized in Table I, which also contains other performance metrics, such as the computational speed and the results variation in consecutive runs. This table presents the results for FL dataset, as well, which is analyzed afterwards.

All methods present a similar BPM accuracy, excepting the M1 method. For instance, it presented a correlation coefficient equal to $r^2 = 0.56$, which clearly indicates a lack of relation between ECG and radar measures. On the other hand, M2 and M3 were the ones that stand out with the best performance, having the highest correlation coefficient $r^2 = 0.99$, the lowest coefficients of variation ($CV = 1.7\%$ and $CV = 1.5\%$) and the lowest limits of agreement. Between both, it should be highlighted the M3 performance in other metrics. For instance, 95% of the dataset presented an error that did not exceed 2.46 BPM, as shown in Fig. 9, while the remain methods present a BPM error superior to 2.6 BPM. In [14] the authors obtained a similar accuracy using the same carrier frequency and transmitted power. Aside from M1, M6 is the one that requires less computational resources. In fact, M6 presents a performance slightly lower than M2 and M3.

Methods that combined wavelets with EEMD (M2 and M5) were specially time consuming, since for each IMF it is required to perform a certain number of repeated observations. Furthermore, EEMD methods presented slightly different results in consecutive runs, probably due to the different characteristics of the noise added on each observation. This could induce an additional error and compromise the results reliability.

The M4 method (using WPD) presented also less satisfactory results, either implemented alone or combined with EEMD. Besides, this method presented a higher execution time, which is related to the nodes decomposition.

Observing now the obtained results for FL dataset (see Table I), the methods with the best performance were M3 and M6, which were the faster either (neglecting the M1 case). However, it is also possible to understand the results impact due to the smaller reflecting areas and lower amplitude motions of subjects 3 and 4. As expected, the error in BPM increased in general, namely between 6 to 8 BPM, excepting for the BPF where an abrupt increase was verified. The correlation coefficient got also worst, as well as the B&A parameters. Even though, the M3 method stands out for being the best method, having the highest correlation coefficient $r^2 = 0.92$, the lowest CV and the lowest run time.

Regarding the second metrics level, the radar peaks position was evaluated in relation to ECG peaks, through the Δ_t parameter. Starting with the SH dataset, Fig. 10 shows an histogram that indicates the peaks location distribution in relation to the ECG peak. For instance, if the Δ_t is equal to $\overline{\text{IBI}}/2$, all bars would be around 0.5. On the other hand, if radar peaks were exactly synchronized with ECG peaks, the histogram bars would only fall around the 0.1 value, and this would be the most preferable situation. Assuming that a constant offset would be acceptable, the bars should lie around any other value, but exclusively that one. In fact, the histogram from Fig. 10 shows us a wider distribution for every

TABLE I
EVALUATION METRICS FOR HEART RATE ACCURACY

Method	Bland & Altman										ϵ (BPM)		Rt (sec)		RMSE	
	r^2		Bias (BPM)		LLoA (BPM)		ULoA (BPM)		CV (%)							
	SH	FL	SH	FL	SH	FL	SH	FL	SH	FL	SH	FL	SH	FL	SH	FL
M1	0.56	0.30	-4.70	-6.10	-20.0	-26.0	10.0	14.0	10.0	14.0	16.80	28.10	0.68	1.04	8.90	11.80
M2	0.99	0.88	0.49	1.80	-2.0	-3.90	3.0	7.50	1.70	3.70	2.60	7.96	242.14	379.34	1.33	3.38
M3	0.99	0.92	0.19	0.80	-2.10	-3.90	2.50	5.50	1.50	3.20	2.46	5.54	10.80	22.78	1.20	2.55
M4	0.97	0.88	-0.47	-0.24	-4.20	-5.90	3.30	5.40	2.50	3.80	4.31	6.28	233.30	400.70	1.95	2.88
M5	0.98	0.89	0.20	1.10	-2.90	-4.40	3.30	6.60	2.0	3.60	3.10	7.58	458.20	758.08	1.57	4.52
M6	0.98	0.90	-0.21	-0.04	-3.10	-5.30	2.60	5.20	1.90	3.50	2.73	6.16	19.40	35.50	1.47	2.66

SH - short-version dataset, FL - full-version dataset, r^2 - Correlation coefficient, Bias - mean difference between ECG and radar BPM, LLoA - Lower limit of agreement, ULoA - Upper limit of agreement, CV - Coefficient of variation, ϵ - Error in BPM reached for 95% of the dataset, Rt - run time in seconds for the error computation, CR - Indicator if the results changed in consecutive runs, RMSE - Root mean square error.

TABLE II
EVALUATION METRICS FOR PEAK LOCATION CONSISTENCY

Method	$\overline{\text{IBI}}$ (ms)		$\sigma_{\overline{\text{IBI}}}$ (ms)		$\overline{\Delta_t}$ (ms)		$\sigma_{\overline{\Delta_t}}$ (ms)	
	SH	FL	SH	FL	SH	FL	SH	FL
M1	950.2	977.9	316.0	356.0	177.4	181.2	74.3	88.8
M2	783.9	780.6	94.4	118.5	173.7	179.3	69.4	85.2
M3	792.8	799.2	103.3	131.3	173.2	178.9	67.4	83.7
M4	801.6	809.9	126.8	152.7	174.3	180.0	73.1	87.8
M5	784.1	784.3	109.4	135.1	175.3	180.7	74.6	88.9
M6	800.3	813.1	116.5	147.6	173.8	179.6	70.4	85.9

SH - short-version dataset, FL - full-version dataset, $\overline{\text{IBI}}$ - average IBI, $\sigma_{\overline{\text{IBI}}}$ - average standard deviation of $\overline{\text{IBI}}$, $\overline{\Delta_t}$ - average time difference between radar and the closest ECG peak, $\sigma_{\overline{\Delta_t}}$ - standard deviation of $\overline{\Delta_t}$

value, which indicates a certain level of variability for all methods.

Table II shows the results of the obtained radar IBI and the Δ_t variation among all methods. From Table II and similarly from Fig. 10, it can be inferred that all methods have a similar behavior and no one stands out in particular. For comparison purposes, the $\overline{\text{IBI}}$ for ECG was equal to 785.72 ms and its $\sigma_{\overline{\text{IBI}}}$ was equal to 37.48 ms. In contrast, the $\overline{\text{IBI}}$ of radar for each method present a somewhat difference in relation to the ECG $\overline{\text{IBI}}$, which is more notorious for the M1 method. However, wider differences can be noticed in the all $\sigma_{\overline{\text{IBI}}}$, which represents a IBI variability higher than expected for the radar side.

These results may be explained with the peak location variation, as suggested by $\overline{\Delta_t}$ results. There is indeed a considerable offset on the radar peak position, and in fact, this offset can be seen as worrisome considering its standard deviation, which varies between 67 and 75 ms. This variation might be translated in an additional error on the IBI determination.

For the FL dataset, the $\overline{\text{IBI}}$ ECG was equal to 789.4 ms and its $\sigma_{\overline{\text{IBI}}}$ was equal to 50.3 ms. The radar $\overline{\text{IBI}}$ results did not altered much, but they became slightly worse for $\sigma_{\overline{\text{IBI}}}$. Likewise, the $\overline{\Delta_t}$ and its $\sigma_{\overline{\Delta_t}}$ increased around 10 ms. Almost all results were affected after adding signals from subjects 3 and 4. In this sense, it is possible to conclude that low amplitude motions hamper even more the methods sensitivity to precisely determine the radar peaks location, which can also compromise the heart rate accuracy.

Thus, we believe that although DWT revealed being the best method for heart rate estimation, it might not be suitable for HRV estimation and all methods presented similar results regarding the peak position consistency. Therefore, the direct computation of HRV parameters might not be possible as it is, and other approaches should be explored. This conclusion in line with Kim *et al.* in [12], where a different radar with a lower carrier frequency was used.

VII. CONCLUSION

In this work, a comparative study for cardiac signal extraction was performed, considering real application scenarios. Six different methods were selected from literature, implemented and compared, considering two main issues: the inter-individual stature variability and non-controlled monitoring environments. The impact of the inter-individual variability in the signals amplitude was observed, but more research is required to understand if the lower amplitude is necessarily related with the subjects' gender or exclusively related with the body statures.

Regarding the performance of the cardiac extraction methods, standalone wavelet-based methods showed to be the more indicated for heart rate estimation, since it presented the smallest error and the fastest computational effort, regardless of the subject's body stature. This was observed for both CWT and DWT, where DWT stand out as being the method with the best performance. However, a results degradation was verified in general, when subjects with lower amplitude motions were included in the dataset.

Additionally, the radar peaks position consistency was evaluated. Although the DWT presented the best accuracy results, there is no guarantee that this method, or any other herein tested, can provide the peak location with enough precision for HRV parameters estimation, at least using the described system setup. The radar $\sigma_{\overline{\text{IBI}}}$ varied largely from the one observed for ECG, as well as $\sigma_{\overline{\Delta_t}}$. This fact can contribute to an additional error in HRV parameters estimation. Therefore, other approaches should be explored to estimate HRV, since the DWT might not be used solely.

ACKNOWLEDGMENT

The authors would like to thank the Research Centre in Digital Services (CISeD) and the Polytechnic of Viseu for their support.

REFERENCES

[1] M. Raja and S. Sigg, "Applicability of RF-based methods for emotion recognition: A survey," in *Proc. IEEE Int. Conf. Pervasive Comput. Commun. Workshops*, Mar. 2016, pp. 1–6.

[2] C. Gouveia, A. Tomé, F. Barros, S. C. Soares, J. Vieira, and P. Pinho, "Study on the usage feasibility of continuous-wave radar for emotion recognition," *Biomed. Signal Process. Control*, vol. 58, Apr. 2020, Art. no. 101835.

[3] S. Pisa, E. Pittella, and E. Piuzzi, "A survey of radar systems for medical applications," *IEEE Aerosp. Electron. Syst. Mag.*, vol. 31, no. 11, pp. 64–81, Nov. 2016.

[4] O. B. Lubecke, V. Lubecke, A. Droitcour, B. Park, and A. Singh, *Doppler Radar Physiological Sensing*. Hoboken, NJ, USA: Wiley, 2015.

[5] C. Gouveia, J. Vieira, and P. Pinho, "A review on methods for random motion detection and compensation in bio-radar systems," *Sensors*, vol. 19, no. 3, p. 604, Jan. 2019.

[6] J. C. Lin, J. Kiernicki, M. Kiernicki, and P. B. Wollschlaeger, "Microwave apexcardiography," *IEEE Trans. Microw. Theory Techn.*, vol. MTT-27, no. 6, pp. 618–620, Jun. 1979.

[7] J. Wang, X. Wang, Z. Zhu, J. Huangfu, C. Li, and L. Ran, "1-D microwave imaging of human cardiac motion: An *ab-initio* investigation," *IEEE Trans. Microw. Theory Techn.*, vol. 61, no. 5, pp. 2101–2107, May 2013.

[8] J. Tu and J. Lin, "Respiration harmonics cancellation for accurate heart rate measurement in non-contact vital sign detection," in *IEEE MTT-S Int. Microw. Symp. Dig.*, Jun. 2013, pp. 1–3.

[9] H. Zhang *et al.*, "The separation of the heartbeat and respiratory signal of a Doppler radar based on the LMS adaptive harmonic cancellation algorithm," in *Proc. 6th Int. Symp. Comput. Intell. Des.*, Hangzhou, China, Oct. 2013, pp. 362–364.

[10] X. Li, B. Liu, Y. Liu, J. Li, J. Lai, and Z. Zheng, "A novel signal separation and de-noising technique for Doppler radar vital signal detection," *Sensors*, vol. 19, no. 21, p. 4751, Nov. 2019.

[11] V. L. Petrović, M. M. Janković, A. V. Lupšić, V. R. Mihajlović, and J. S. Popović-Bovović, "High-accuracy real-time monitoring of heart rate variability using 24 GHz continuous-wave Doppler radar," *IEEE Access*, vol. 7, pp. 74721–74733, 2019.

[12] J.-Y. Kim, J.-H. Park, S.-Y. Jang, and J.-R. Yang, "Peak detection algorithm for vital sign detection using Doppler radar sensors," *Sensors*, vol. 19, no. 7, p. 1575, Apr. 2019.

[13] S. Suzuki, T. Matsui, S. Gotoh, Y. Mori, B. Takase, and M. Ishihara, "Development of non-contact monitoring system of heart rate variability (HRV)—An approach of remote sensing for ubiquitous technology," in *Proc. Int. Conf. Ergonom. Health Aspects Work Comput.* Berlin, Germany: Springer, 2009, pp. 195–203.

[14] C. Li, Y. Xiao, and J. Lin, "Design guidelines for radio frequency non-contact vital sign detection," in *Proc. 29th Annu. Int. Conf. IEEE Eng. Med. Biol. Soc.*, Aug. 2007, pp. 1651–1654.

[15] S. Tomii and T. Ohtsuki, "Heartbeat detection by using Doppler radar with wavelet transform based on scale factor learning," in *Proc. IEEE Int. Conf. Commun. (ICC)*, Jun. 2015, pp. 483–488.

[16] I. Mostafanezhad, E. Yavari, O. Boric-Lubecke, V. M. Lubecke, and D. P. Mandic, "Cancellation of unwanted Doppler radar sensor motion using empirical mode decomposition," *IEEE Sensors J.*, vol. 13, no. 5, pp. 1897–1904, May 2013.

[17] F. Weishaupt, I. Walterscheid, O. Biallawons, and J. Klare, "Vital sign localization and measurement using an LFMCW MIMO radar," in *Proc. 19th Int. Radar Symp. (IRS)*, Bonn, Germany, Jun. 2018, pp. 1–8.

[18] W. Hu, Z. Zhao, Y. Wang, H. Zhang, and F. Lin, "Noncontact accurate measurement of cardiopulmonary activity using a compact quadrature Doppler radar sensor," *IEEE Trans. Biomed. Eng.*, vol. 61, no. 3, pp. 725–735, Mar. 2014.

[19] Y. I. Jang, J. Y. Sim, J.-R. Yang, and N. K. Kwon, "The optimal selection of mother wavelet function and decomposition level for denoising of DCG signal," *Sensors*, vol. 21, no. 5, p. 1851, Mar. 2021.

[20] M. Li and J. Lin, "Wavelet-transform-based data-length-variation technique for fast heart rate detection using 5.8-GHz CW Doppler radar," *IEEE Trans. Microw. Theory Techn.*, vol. 66, no. 1, pp. 568–576, Jan. 2018.

[21] T. K. V. Dai *et al.*, "Enhancement of remote vital sign monitoring detection accuracy using multiple-input multiple-output 77 GHz FMCW radar," *IEEE J. Electromagn., RF Microw. Med. Biol.*, vol. 6, no. 1, pp. 111–122, Mar. 2022.

[22] S. Laborde, E. Mosley, and J. F. Thayer, "Heart rate variability and cardiac vagal tone in psychophysiological research–recommendations for experiment planning, data analysis, and data reporting," *Frontiers Psychol.*, vol. 8, p. 213, Feb. 2017.

[23] A. LoMauro and A. Aliverti, "Sex differences in respiratory function," *Breathe*, vol. 14, no. 2, pp. 131–140, Jun. 2018.

[24] L. Liu, W. Xiao, J. Wu, and S. Xiao, "Wavelet analysis based noncontact vital signal measurements using mm-Wave radar," in *Proc. Int. Conf. Green, Pervas., Cloud Comput.* Cham, Switzerland: Springer, 2020, pp. 3–14.

[25] A. Graps, "An introduction to wavelets," *IEEE Comput. Sci. Eng.*, vol. 2, no. 2, pp. 50–61, Jun. 1995.

[26] C. Gargour, M. Gabrea, V. Ramachandran, and J. M. Lina, "A short introduction to wavelets and their applications," *IEEE Circuits Syst. Mag.*, vol. 9, no. 2, pp. 57–68, 2nd Quart., 2009.

[27] J. Kevric and A. Subasi, "Comparison of signal decomposition methods in classification of EEG signals for motor-imagery BCI system," *Biomed. Signal Process. Control*, vol. 31, pp. 398–406, Jan. 2017.

[28] N. E. Huang *et al.*, "The empirical mode decomposition and the Hilbert spectrum for nonlinear and non-stationary time series analysis," *Proc. Roy. Soc. London Ser. A, Math., Phys. Eng. Sci.*, vol. 454, no. 1971, pp. 903–995, Mar. 1998.

[29] G. Wang, X.-Y. Chen, F.-L. Qiao, Z. Wu, and N. E. Huang, "On intrinsic mode function," *Adv. Adapt. Data Anal.*, vol. 2, no. 3, pp. 277–293, Jul. 2010.

[30] Z. Wu and N. E. Huang, "Ensemble empirical mode decomposition: A noise-assisted data analysis method," *Adv. Adapt. Data Anal.*, vol. 1, no. 1, pp. 1–41, Jan. 2009.

[31] C. Gouveia, D. Albuquerque, J. Vieira, and P. Pinho, "Dynamic digital signal processing algorithm for vital signs extraction in continuous-wave radars," *Remote Sens.*, vol. 13, no. 20, p. 4079, Oct. 2021.

[32] J.-G. Kim, S.-H. Sim, S. Cheon, and S. Hong, "24 GHz circularly polarized Doppler radar with a single antenna," in *Proc. Eur. Microw. Conf.*, vol. 2, 2005, p. 4.

[33] D. Batista, H. Plácido da Silva, A. Fred, C. Moreira, M. Reis, and H. A. Ferreira, "Benchmarking of the BITalino biomedical toolkit against an established gold standard," *Healthcare Technol. Lett.*, vol. 6, no. 2, pp. 32–36, Apr. 2019.

[34] B.-K. Park, V. Lubecke, O. Boric-Lubecke, and A. Host-Madsen, "Center tracking quadrature demodulation for a Doppler radar motion detector," in *IEEE MTT-S Int. Microw. Symp. Dig.*, Jun. 2007, pp. 1323–1326.

[35] B.-K. Park, O. Boric-Lubecke, and V. M. Lubecke, "Arctangent demodulation with DC offset compensation in quadrature Doppler radar receiver systems," *IEEE Trans. Microw. Theory Techn.*, vol. 55, no. 5, pp. 1073–1079, May 2007.

[36] P. Kathirvel, M. S. Manikandan, S. R. M. Prasanna, and K. P. Soman, "An efficient R-peak detection based on new nonlinear transformation and first-order Gaussian differentiator," *Cardiovascular Eng. Technol.*, vol. 2, no. 4, pp. 408–425, 2011.
[37] D. Giavarina, "Understanding bland Altman analysis," *Biochem. Med.*, vol. 25, pp. 141–151, Sep. 2015.
[38] R. Klein. *Bland-Altman and Correlation Plot*. MATLAB Central File Exchange. Accessed: Jan. 2022. [Online]. Available: https://www.mathworks.com/matlabcentral/fileexchange/45049-bland-altman-and-correlation-plot

C. Gouveia (Student Member, IEEE) received the Licenciatura degree in health equipment technologies from the Polytechnical Institute of Leiria, Portugal, in 2011, and the Licenciatura and master's degrees in electronics and telecommunication engineering from the University of Aveiro, Portugal, in 2017, where she is pursuing the Ph.D. degree in electrical engineering. Nowadays, she is a Researcher with the Radio Systems Group, Instituto de Telecomunicações (IT), Aveiro, Portugal. She focused in non-contact vital signs acquisition using radar systems. Her research work led to five journal articles and three international conferences. She received the Prize ANACOM-URSI Portugal in 2021, the EuMA First Prize at the Young Scientist Contest in MIKON Conference 2020, and the Second Award Fraunhofer Portugal Challenge in 2018. She was involved in the research project TexBoost: less commodities more specialities, which aimed to develop a smart seat cover and integrating a bio-radar systems. This project led to a patent submission.

D. Albuquerque received the Diploma degree in electronics and telecommunications engineering and the Ph.D. degree in electrical engineering from the University of Aveiro, Portugal, in 2007 and 2013, respectively. From 2011 to 2013, he was an Assistant Lecturer with the School of Technology and Management of Viseu, Polytechnic Institute of Viseu, where he was a Visiting Professor from 2013 to 2019 and has been an Assistant Professor since 2019. His main research interest is in the development of signal processing tools to location and radar systems. He is a member of the Center for Research in Digital Services (CISeD). He receives the Prize ANACOM-URSI Portugal in 2021, First Plug Prize from APRITEL in 2010, and the Third Prize in Technological Realization in Audio Engineering from the Portuguese Section of Audio Engineering Society in 2007.

P. Pinho (Senior Member, IEEE) was born in Vale de Cambra, Portugal, in 1974. He received the Licenciado and master's degrees in electrical and telecommunications engineering and the Ph.D. degree in electrical engineering from the University of Aveiro in 1997, 2000, and 2004, respectively. He is currently an Assistant Professor with the Electronics, Telecommunications and Informatics Engineering Department, University of Aveiro (UA), and a Senior Member of the Research Staff with the Instituto de Telecomunicações (IT), Aveiro, Portugal. He has authored or coauthored one book, ten book chapters, and more than 100 papers for conferences and international journals. He participated as a principal investigator or a coordinator in projects with scientific and/or industry focus, both at the national and international level. To date, he has led and leads eight Ph.D. students and 60 M.Sc. students. His current research interest is in optical systems and antennas. He serves as a technical program committee member in several conferences, a reviewer of several IEEE journals, and a member of IEEE APS.

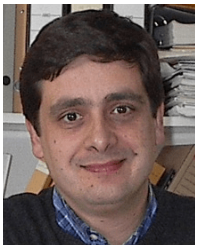

J. Vieira received the B.Sc. degree in electrical engineering and the M.Sc. degree in systems and automation from the University of Coimbra, Portugal, in 1988 and 1993, respectively, and the Ph.D. degree in electrical engineering from Aveiro University, Portugal, in 2000. Since then, he has been an Assistant Professor with Aveiro University. In 2004, he founded the AES Portuguese Section, where he was the President from 2005 to 2011. His main research interests are digital audio signal processing, ultrasonic location, software defined radio, all-digital radio front-ends, and radar. In 2010, he won the Plug Award from APRITEL with the "Bio-inspired cochlear radio."